

In situ tunneling measurements in a transmission electron microscope on nanomagnetic tunnel junctions

J. W. Lau,^{1,a)} P. Morrow,¹ J. C. Read,¹ V. Höink,¹ W. F. Egelhoff,¹ L. Huang,² and Y. Zhu²

¹National Institute of Standards and Technology, Gaithersburg, Maryland 20899, USA

²Department of Condensed Matter Physics and Materials Science, Brookhaven National Laboratory, Upton, New York 11973, USA

(Received 5 April 2010; accepted 15 May 2010; published online 30 June 2010)

We showed that a chain of nanomagnetic tunnel junctions (MTJs) devices can be electrically addressed individually, *in situ*, in a transmission electron microscope, such that transport properties can be in principle, quantitatively correlated with each device's defects and microstructure. A unique energy barrier was obtained for each device measured. Additionally, *in situ* tunneling magnetoresistance (TMR) measurements were obtained for a subset of devices. We found that TMR values for our nano-MTJs were generally smaller than TMR in the unpatterned film. © 2010 American Institute of Physics. [doi:10.1063/1.3446841]

Magnetic tunnel junctions (MTJs) are keystone components in technologies such as read heads in hard drives, magnetic sensors, and magnetoresistive random access memories. During manufacturing, various processes produce defects that cause nonuniform behaviors in these nanometer-size MTJ arrays. Defects such as pinholes and hot spots can fundamentally change the tunneling barrier characteristics and ultimately cause them to fail. Junction morphologies and stack microstructures have been compared in cross-section transmission electron microscopy (TEM) between films with good and poor tunneling magnetoresistance (TMR).^{1,2} The challenge remains in isolating defects that cause poor performance. Others have developed scanning-tunneling type measurements to image current density directly in efforts to locate the relevant defects.^{3,4} While these methods do pinpoint the locations of anomalous behavior, the extraction of such regions for further study is not straightforward. Recently, Petford-Long and co-workers demonstrated that *in situ* tunneling experiment can be done in a TEM, on a film cross-section consisting of two ferromagnetic electrodes separated by an insulator.^{5,6} The scope of the present work expands on this technique, applying it for the first time, to a series of fully operational, $\sim 100 \times 150 \text{ nm}^2$ MTJs. The motivations for making 100 nm devices are twofold. First, these dimensions are relevant to devices of practical application as discussed earlier. Second, by restricting the current flow through constricted dimensions, it makes quantitative comparison between adjacent devices feasible. We have achieved, for the first time, *in situ* TMR measurements on isolated nanodevices that are part of a TEM sample.

The MTJ was dc magnetron sputtered onto low-resistivity ($0.001 \text{ } \Omega \text{ cm}$) [100] silicon substrate. The stack sequence is Cr 50/Ta 3/IrMn 10/CoFe 4/Ru 0.85/CoFeB 4/Mg 0.4/MgO 1.5/CoFeB 2.5/Ta 8/Ru 7 (all numbers in nanometer). Throughout this manuscript, the notations "pinned" and "free" layer refer to the 4 nm and 2.5 nm CoFeB layers, respectively. The 4 nm of CoFe was built-in to balance the stray field from the pinned layer.

Prior to the MTJ deposition, the silicon's native oxide was stripped in a buffered oxide etch (6:1 $\text{NH}_4\text{F}:\text{HF}$) and

the wafer was placed immediately into the sputter chamber. A 60 s Ar presputter was done prior to the deposition of the Cr layer. Upon removing the film from the deposition chamber, a pinning field (60 mT at $280 \text{ }^\circ\text{C}$, 1 min) was applied to pin the CoFe to IrMn along one of the Si [100] directions. The entire structure was annealed in a 60 mT field for 15 min at $315 \text{ }^\circ\text{C}$. Current-in-plane tunneling (CIPT) measurements on this film indicated 32% TMR, and a resistance-area (RA) product of $1160 \text{ } \Omega \text{ } \mu\text{m}^2$.

Figure 1(a) is a schematic representation of an array of $100 \times 400 \text{ nm}^2$ stripes with 300 nm spacing all around patterned with e-beam lithography. The lengths of the stripes were aligned parallel to the pin direction. The pattern was transferred subtractively through an e-beam evaporated TaC mask with a 500 W Ar plasma. In anticipation of the focused Ga^+ ion beam damage (FIB, our next process step), the post-patterned region was backfilled with $1 \text{ } \mu\text{m}$ of SiO_2 . From here, the sample was thinned to electron transparency perpendicular to the stripe direction by a combination of mechanical polishing and FIB, as discussed in Ref. 5.

However, the possibility of Ga penetration into the MTJ stack can alter our data interpretation, or worse, short our junctions altogether. We deliberately stopped FIB milling at 300 nm because it was showed by SRIM simulations⁷ that Ga^+ implantation at a milling energy of 30 keV can penetrate into the MTJ side wall, up to 50 nm on each polished surface. Instead, we continued thinning to the target thickness with a 500 W Ar plasma. At this point, several nanometer of the

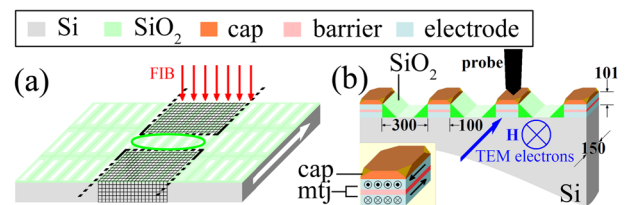


FIG. 1. (Color online) Schematic representation of (a) MTJ stack after patterning into $100 \times 400 \text{ nm}^2$ stripes and backfilled with SiO_2 . White arrow on the side of the slab shows pinning direction. Dark regions are removed by mechanical polishing and FIB. (b) Enlargement of circled region in (a), showing the probe, electron beam, magnetic field, and pinned and free layer geometries in reference to the specimen position. Beam entrance surface is the magnetic north. All numbers have units of nanometer.

^{a)}Electronic mail: june.lau@nist.gov.

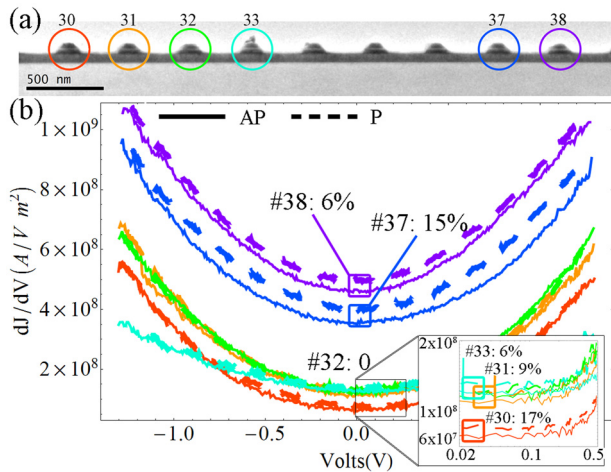


FIG. 2. (Color online) Image shows devices 30 through 38. The color coded circles correspond to the device specific conductance (dI/dV vs V) curves. The conductances are normalized by the junction areas. Solid and dotted curves correspond to AP and P configuration, respectively. The inset is an enlargement of the boxed low-voltage bias region where the voltage is plotted in log scale.

SiO_2 sputtered on previously as a FIB protection, remained on top of the TaC caps, which were the intended points of electrical contact. This residual SiO_2 was removed with a 200 W $\text{CHF}_3 + \text{O}_2$ plasma for 1 min at a time, until it was gone.

Figure 2(a) is an image showing part of the device chain. The devices are enumerated from 1 to 50. The final sample thickness ranged from 146 to 172 nm along the TEM beam direction as determined by electron energy loss spectroscopy (EELS). The device lengths were between 92 and 117 nm. Figure 1(b) shows schematically the specimen position, beam direction, external magnetic field direction (when applied), contacting probe, and the pinned and free layers of the MTJs (inset). Even though the schematic shows that the bottom-pinned layer as parallel to the beam direction, this is not necessarily the case as this orientation is entirely dependent on how the specimen was loaded in the microscope. The orientation is not particularly important for reasons to be discussed shortly.

The transport measurements were made possible by a nonstandard TEM specimen holder with a built-in piezotube [Fig. 3(a)]. A voltage biased sample was held fixed to the specimen holder while a grounded PtIr wire attached to the piezotube, made contact to one junction at a time. Figure 3(b) shows the probe approaching the device region. Figure 3(c) is a higher magnification view of the tip making contact with one of the MTJs. The tip radius is significantly larger

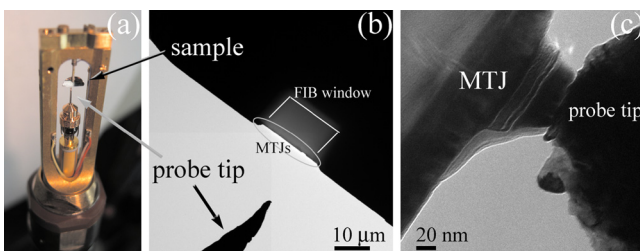


FIG. 3. (Color online) (a) TEM holder with a probe mounted on a built-in piezotube. (b) Probe approaching devices region. (c) Contact is established with one of the MTJs.

than the devices; however the devices are spaced far enough apart that the tip can only touch one device at a time. At the point of contact, a flow of material was observed at the tip making the appearance of a uniform and smooth contact.

The transport measurements took place in a nearly zero-field TEM specifically designed for magnetic studies. The direction of the pinned layer was designed to align with the optic axis of the microscope. In the absence of an external magnetic field, we expect the ferromagnetic layers to be in the antiparallel (AP) configuration, along the optic axis due to the magnetostatic interaction between the pinned and free layers. This was verified, in the ideal geometry, with micromagnetics simulation;⁸ though we cannot rule out the possibility that the pinned and free layers may not be perfectly AP due to the tapered edges and other defects.

Some measurements however, were made also in the parallel (P) configuration in order to determine TMR. P alignment was achieved by switching either the free or pinned ferromagnetic layer using the objective lens of the microscope. While this microscope operates principally in a minimal field region, it is possible to over-excite the objective lens to produce a magnetic field along the optic axis. The region of operation up to 50 mT had been previously calibrated.⁹ We know from the CIPT measurements that 40 mT was large enough to switch the pinned layer. Therefore, the MTJ should be in the P configuration at 40 mT, regardless whether the pinned or the free layer switched. Thus it was unnecessary to track which layer actually switched during the experiment. We ran the objective lens at a 50 mT field for the current versus voltage (IV) curves taken in the P configuration.

Figure 2(b) shows a family of six conductance (dI/dV , normalized to junction area) curves taken from the corresponding devices in Fig. 2(a). The solid and dotted curves correspond to the device in the AP and P configuration, respectively. These curves are non-ohmic, which is what one might expect from tunnel junctions. Based on the measured RA product in this film prior to patterning, we expected a near zero-bias resistance of 116 k Ω in devices of these dimensions in the P state. A linear fit of the P state IV curves in the “low-voltage” range of $-0.1 \text{ V} \leq V \leq 0.1 \text{ V}$ gave us the resistances of individual devices. The average resistance was $465 \pm 120 \text{ k}\Omega$ (120 k Ω =1 standard deviation). Most of these resistance values were higher than the expected 116 k Ω ; this indicates that none of our junctions were shorted. Taking the definition of TMR as $(R_{AP} - R_P)/R_P$, where R_{AP} and R_P are the linear fits of the AP and P state IV curves in the low-voltage regime, we obtain TMR values for device number 30, 31, 32, 33, 37, and 38 as 17.1%, 8.8%, 0, 5.6%, 15.3%, and 5.5%, respectively. Even though we had measured 32% TMR in this same film prior to patterning, the TMR effect is smaller in these nanometer size junctions.

Using the Simmons formalism on the electric tunneling effect with similar electrodes,¹⁰ and assuming a constant effective barrier width (thickness of the MgO film), s of 1.14 nm, we obtained the average energy barrier ϕ of our devices as 1.09 eV ($\pm 0.07 \text{ eV}$ =1 standard deviation) from the collection of IV measurements acquired at a maximum bias of 0.5 V. For $|V| \leq \phi/e$, we used dI/dV of the Simmons model shown in Eq. (1) as our fit function. Here, a is the junction area, e is the electron charge and V is the bias voltage. $A = (4\pi s/h)\sqrt{2m}$ (h and m are the Planck constant and electron

mass, respectively) and $J_0 = e/2\pi\hbar s^2$. In order to calculate the current density J , we needed to know a , the area of the junctions; this we measured with bright-field TEM images and EELS

$$\frac{dI}{dV} = \exp\left\{-As\sqrt{\varphi - \frac{eV}{2}}\right\} \left\{-\frac{aJ_0e}{2} + \frac{aJ_0eAs}{4}\sqrt{\varphi - \frac{eV}{2}}\right\} + \exp\left\{-As\sqrt{\varphi + \frac{eV}{2}}\right\} \left\{-\frac{aJ_0e}{2} + \frac{aJ_0eAs}{4}\sqrt{\varphi + \frac{eV}{2}}\right\}. \quad (1)$$

Since this was a series of two-point measurements, it was important to find a MTJ stack recipe with a large enough RA value such that the sum of all the resistances in series is insignificant in comparison to that of the MgO junction. Nonetheless, we estimated the total series resistance by considering all possible sources. We had a list of at least ten different sources of resistance in the circuit; other than the junction, major contribution to the voltage drop was expected from the contact, the low-resistivity Si, and the carbon paint that bonds the Si substrate to the TEM grid. We estimated 1 k Ω minimum circuit resistance. The measured circuit resistance was 2 k Ω ; discussion of this measurement is in the next section.

In the course of our measurements, we sacrificed five devices in order to see how they break. In total, 17 devices were probed. All seventeen devices survived a maximum bias voltage of 0.5 V. Surviving means that the same device can reproduce the same IV trace with 0.5 V bias repeatedly. 15 devices survived 1 V and eleven survived 1.5 V. We put 2 V or more on five devices; of the five, two survived 2 V and none survived 3 V. The dead devices were not completely broken in that at the 2–3 V range, we never saw short circuits; instead we saw an order of magnitude current surge, but still non-Ohmic behavior. We continued to increase bias voltage until the junctions were bypassed altogether, and the IV traces were linear. In the region between 5 and 6 V, we measured a resistance of 2 k Ω . We take this value to be the total series resistance, less the MgO junction, for the entire circuit. This value is comparable to our 1 k Ω estimate. Therefore, we subtracted the 2 k Ω circuit resistance from all IV curves to better represent the junctions. All five junctions that we biased above 2 V failed in a similar way. The low-voltage ($-0.1 \text{ V} \leq V_b \leq 0.1 \text{ V}$) resistances recorded after junction failure were between 28 and 38 k Ω .

One reason why the average measured resistance value was larger than the anticipated value based on RA product may be that the conducting parts of the MTJ pillars are smaller than the physical dimension of the structures. A straightforward explanation is oxidation of edges and surfaces of the metallic components as well as the Si substrate. The oxidation of the ferromagnetic electrodes may also play a role in the observed reduction in TMR.

A barrier height of 1.09 eV agrees well with measurements from a similar system.¹¹ We arrived at this number by assuming that the MgO thickness is constant throughout the

devices. Using a much thinner segment of the same sample, we found that the MgO thickness is typically between 1.1 and 2.0 nm. With the Simmons model, the best fit for φ was obtained by assuming $s = 1.14 \text{ nm}$, which is slightly less than the average measured MgO thickness. Others have encountered the similar problem of s from fit being smaller than the expected s when using a more advanced electric tunneling model.¹² Those authors attributed the poor match between fitted s and the actual MgO thickness to the existence of a distribution of barrier thicknesses within their MTJs; a fact was evident in our MTJs as well. Therefore, accurate description of tunneling phenomenon may require a more sophisticated model as suggested by the previous authors.

We have measured TMR, in addition to the junction energy barrier, for the first time on fully functional nano-MTJs built into a TEM sample. Since we know exactly which junction is engaged at a given time, information regarding the physical size of the junction and its morphology is readily available. Furthermore, since no more specimen preparation is needed, in principle, after the transport measurements, we can be certain that all of the structural causes to a particular set of IV characteristics are self-contained. Here lies the primary strength of this technique. While the initial experimental setup took several hours, a fast throughput, up to one device per minute, is possible. From these measurements, we determined an average value of 1.09 eV for φ assuming an effective barrier width of 1.14 nm on a handful of nominally identical devices. The average TMR value of 8.7% was somewhat lower than the 32% recorded in same sample just prior to patterning. This was possibly due to edges and surfaces damages or oxidation during the nanopatterning process.

The authors acknowledge the illuminating discussions with Dr. Joshua Pomeroy. Much appreciated film growth assistance was provided by Dr. P. J. Chen and Mr. Audie Castillo. This research was performed in part at the NIST Center for Nanoscale Science and Technology.

¹J. Hayakawa, S. Ikeda, Y. M. Lee, F. Matsukura, and H. Ohno, *Appl. Phys. Lett.* **89**, 232510 (2006).

²J. J. Cha, J. C. Read, W. F. Egelhoff, P. Y. Huang, H. W. Tseng, Y. Li, R. A. Buhrman, and D. A. Muller, *Appl. Phys. Lett.* **95**, 032506 (2009).

³Y. Ando, H. Kameda, H. Kubota, and T. Miyazaki, *Jpn. J. Appl. Phys., Part 2* **38**, L737 (1999).

⁴K. M. Bhutta, J. Schmalhorst, and G. Reiss, *J. Magn. Magn. Mater.* **321**, 3384 (2009).

⁵A. N. Chiamonti, L. J. Thompson, W. F. Egelhoff, B. C. Kabius, and A. K. Petford-Long, *Ultramicroscopy* **108**, 1529 (2008).

⁶A. N. Chiamonti, D. K. Schreiber, W. F. Egelhoff, D. N. Seidman, and A. K. Petford-Long, *Appl. Phys. Lett.* **93**, 103113 (2008).
<http://www.srim.org>.

⁸M. J. Donahue and D. G. Porter, National Institute of Standards and Technology Interagency Report No. NISTIR 6376, 1999 (unpublished).

⁹J. W. Lau, M. A. Schofield, and Y. Zhu, *Ultramicroscopy* **107**, 396 (2007).

¹⁰J. G. Simmons, *J. Appl. Phys.* **34**, 1793 (1963).

¹¹S. P. Parkin, C. Kaiser, A. Panchula, P. M. Rice, B. Hughes, M. Samant, and S. H. Yang, *Nature Mater.* **3**, 862 (2004).

¹²C. W. Miller, Z. P. Li, I. K. Schuller, R. W. Dave, J. M. Slaughter, and J. Akerman, *Phys. Rev. B* **74**, 212404 (2006).